

Research Article

Carbon dioxide as working fluid for medium and high-temperature concentrated solar thermal systems

Van Duong and Gerardo Diaz *

School of Engineering, University of California - Merced, 5200 North Lake Road, Merced, CA 95343, USA

* **Correspondence:** Email: gdiaz@ucmerced.edu; Tel: +1-209-228-7858; Fax: +1-209-228-4047.

Abstract: This paper explores the benefits and drawbacks of using carbon dioxide in solar thermal systems at medium and high operating temperatures. For medium temperatures, application of CO₂ in non-imaging-optics based compound parabolic concentrators (CPC) combined with evacuated-tube collectors is studied. These collectors have been shown to obtain efficiencies higher than 40% operating at around 200°C without the need of tracking. Validated numerical models of external compound parabolic concentrators (XCPCs) are used to simulate their performance using CO₂ as working fluid. For higher temperatures, a mathematical model is implemented to analyze the operating performance of a parabolic trough solar collector (PTC) using CO₂ at temperatures between 100°C and 600°C.

Keywords: solar thermal systems; parabolic troughs; compound parabolic concentrators; medium; high temperature collectors

1. Introduction

The fluctuation in the cost of fuel prices, the increasing demand for energy, and the evident signs of climate change, have fostered the development of technologies that utilize renewable energy sources. Concentrated solar thermal systems continue to be one of the most attractive options to produce power to meet utility-scale needs in certain regions of the U.S. However, in order to reduce levelized cost of solar power, solar thermal systems that can operate at higher temperatures, i.e. 450–600 °C, while remaining thermally stable, are needed.

Previous studies have based improvements of solar thermal system performance by configuring the structure of solar collectors, adjusting the selective coating for higher absorptivity, or preventing

heat loss from the collectors. More recently, studies have based improvements of solar thermal systems performance by experimenting with different working fluids such as ammonia, air, silicon oil and organic working fluids. However, there are downfalls to using these fluids. Working fluids, such as CFC113, CFC114 and CFC11 can deplete the ozone layer [1], so they have been phased out. In addition, ammonia is a health hazard, air has poor thermophysical properties, and silicon oil's high viscosity made it difficult to handle at low temperatures.

There are a few studies that have been conducted considering carbon dioxide (R-744) as the working fluid. Carbon dioxide has a high volumetric capacity, heat transfer coefficients tend to be higher than for other fluids, it is readily available, and it is thermally stable for a wide range of temperatures. Carbon dioxide has a critical pressure and temperature of 7.38 MPa and 31.1 °C, respectively, which is lower than other working fluids. In addition, it is abundant in nature, non-toxic, non-flammable and environmentally safe. This makes carbon dioxide a good candidate for a working fluid in advanced solar thermal systems [1-4]. CO₂ is a greenhouse gas when released to the atmosphere but its global warming potential index is far lower than other working fluids.

Non-imaging-optics based external compound parabolic concentrating reflectors (XCPC) combined with evacuated-tube collectors featuring a metal absorber and a glass-to-metal seal have been shown to obtain efficiencies higher than 40 % operating near 200 °C without the need of tracking [5, 6]. However, these results have been obtained using thermal oil (Duratherm 600) and there is very little information of the performance using alternative working fluids such as CO₂. Yamaguchi et al. [2] carried out an experimental study of solar energy powered Rankine cycle using supercritical CO₂. They found an estimated power generation efficiency of 0.25 and heat recovery efficiency of 0.65.

For higher temperatures, parabolic trough concentrators (PTC) with an absorber inside an evacuated-tube have been simulated and experimentally tested with operating temperatures up to 400 °C using thermal oils such as silicon oil, biphenyl/diphenyl ether (VP-1) and Syltherm 800. Temperatures up to 500 °C have been reached using steam [7-10]. Above 400 °C, the properties of thermal oils degrade significantly causing molecular bond breakdown, excessive system pressure, and an increase in viscosity that can reduce heat transfer efficiency [7, 11]. In addition, thermal oils can be costly and dangerous due to their high flammability and toxicity [7, 9]. Steam as working fluid produced equivalent results compared to thermal oils, however, water can only be used above 0 °C and has to be operated under high working pressure.

This paper presents numerical simulations of XCPC and PTC collectors operating with CO₂ as a working fluid for a range of temperatures that covers the medium and high range.

2. Medium Temperature: XCPC

The mathematical model of the XCPC used to simulate the performance of CO₂ under medium temperatures followed the analysis performed by Tovar-Fonseca [12]. A sketch of the XCPC concentrator and the evacuated tube collector is shown in Figure 1. The collector consists of a glass envelope that has a metal absorber inserted inside that acts as a fin contouring a coaxial pipe. A selective coating is applied to the exterior of the copper-fin absorber. One end of the glass tube is rounded, as shown in Figure 2, and the other end consists of a glass to metal seal that is used to ensure that the vacuum inside the glass tube is not lost. The coaxial pipes consist of concentric external and internal copper pipes with the inlet fluid to the collector flowing in the interior pipe and

the exit fluid flowing in the annulus formed between the two pipes. The absorber fin and the external copper pipe are welded together, so the heat reaching the absorber fin is transferred by conduction to the external pipe that transfers the heat to the working fluid by heat convection. The input dimensions and properties used to simulate the XCPC collector are shown in Table 1.

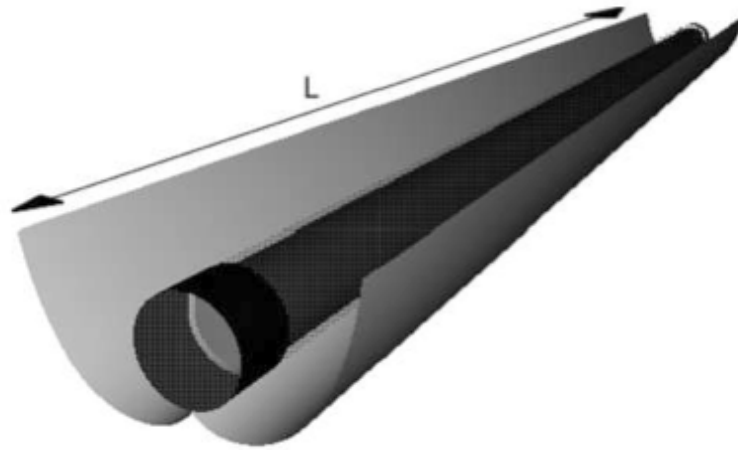


Figure 1. Sketch of XCPC with an absorber [12].

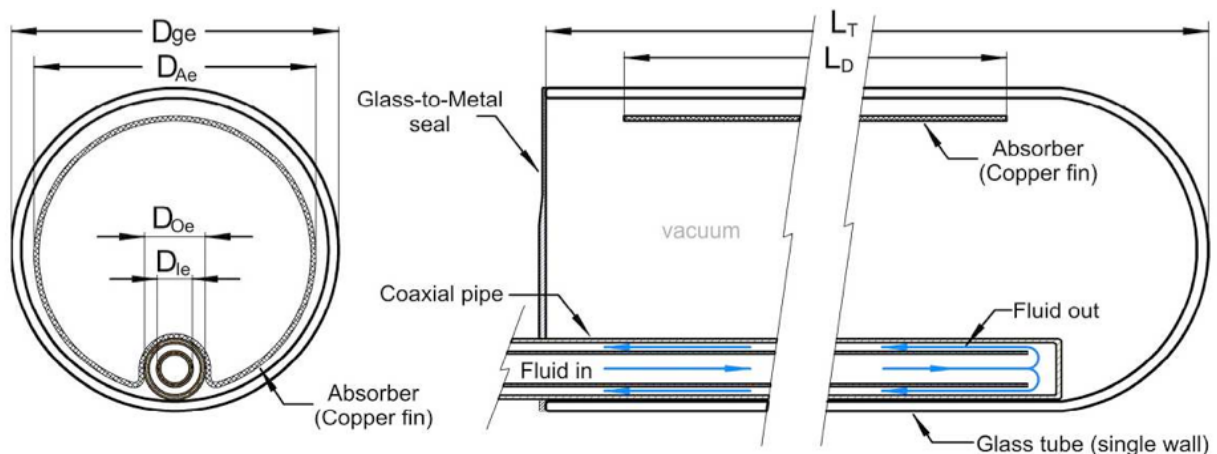


Figure 2. Detailed schematic of the evacuated glass tube with metal absorber and glass-to-metal seal [12].

Table 1. Properties and Dimensions for XCPC with Metal Absorber.

Component	Material	Symbol	Value
Glass tube	Pyrex 7740		
Outer diameter		D_{ge}	65 mm
Inner diameter		D_g	61 mm
Thermal Conductivity		k_g	1.4 W/m·K
Emissivity		ε_g	0.92

Metal absorber/fin	Copper		
Outer diameter		D_{Ae}	56 mm
Thickness		t_0	1 mm
Effective length		L_D	1,640 mm
Absorptivity		α_A	0.95
Emissivity		ε_A	0.01
Selective coating	Metal aluminum nitride cermet		
Thermal conductivity		k_A	200 W/m·K
Coaxial pipes	Copper		
External pipe, outer diameter		D_{Oe}	30 mm
External pipe, inner diameter		D_o	26.6 mm
Internal pipe, outer diameter		D_{Ie}	8 mm
Internal pipe, inner diameter		D_I	6 mm
Hydraulic diameter		D_h	3.5 mm
Thermal conductivity		k_{Cu}	320 W/m·K

2.1. Mathematical Model of XCPC Collector

A mathematical model to represent the XCPC collector was implemented using the thermal analysis in [12, 13] which was implemented in Engineering Equation Solver (EES) [14] to simulate the behavior of CO₂ as the working fluid.

The following assumptions were made: uniform heat flux on absorber, incompressible fluid, constant properties of fluid, constant heat transfer coefficients, negligible fouling factor, negligible potential and kinetic energy changes, and fully developed conditions.

2.1.1. Evacuated Glass Tube

An energy balance applied to the glass cover is given by:

$$\alpha_g G_c + \frac{1}{\frac{1}{\varepsilon_A} + \frac{1 - \varepsilon_g}{\varepsilon_g} \left(\frac{D_{Ae} + t_0}{D_g} \right)} \sigma (T_A^4 - T_g^4) - h_0 (T_g - T_\infty) - \varepsilon_g \sigma (T_g^4 - T_{sky}^4) = 0 \quad (1)$$

where α_g is the absorption coefficient of the glass, and G_c is the irradiance incident on the metal absorber ($G_c = \text{Total irradiance incident on concentrator aperture} \times \text{Concentration ratio} = G_s \times C_{max}$). T_A is the temperature of the absorber, T_g is the temperature at the glass, T_∞ is the temperature of the ambient air, and σ is the Stefan-Boltzmann constant. T_{sky} is the sky temperature and can be related to the ambient temperature by $T_{sky} = 0.0552 T_\infty^{1.5}$ [15]. h_0 is the convection heat transfer coefficient between the outside exterior of the glass and the ambient air, and is given by the empirical equation: $h_0 = 2.8 + 3v$, where v is the velocity of the ambient air nearby the surface of the exterior glass [12, 15]. Finally, ε_g is the emissivity of the glass, ε_A is the emissivity of the absorber, D_{Ae} is the outer diameter of the metal absorber, D_g is the inner diameter of the external glass, and t_0 is the thickness of the metal absorber.

2.1.2. Absorber

The energy balance applied to the absorber gives the following equation:

$$\frac{\alpha_A \tau_g}{1 - (1 - \alpha_A) \rho_g} G_c - \frac{1}{\frac{1}{\epsilon_A} + \frac{1 - \epsilon_g}{\epsilon_g} \left(\frac{D_{Ae} + t_0}{D_g} \right)} \sigma (T_A^4 - T_g^4) - q''_{cond} = 0. \quad (2)$$

α_A is the absorptivity of the absorber, and τ_g and ρ_g are the glass transmissivity and reflectivity, respectively. Performing an energy balance at the absorber fin, the expression for the temperature of the fin as a function of the arc length is given by

$$\frac{T - T_\infty - S/U_L}{T_b - T_\infty - S/U_L} = \frac{\cosh(mx)}{\cosh(m\pi D_{Ae}/2)} \quad (3)$$

where $S = \kappa G_s$, $m = \sqrt{(U_L/t_0/k_A)}$, κ is the absorption coefficient of the absorber fin, t_0 is the thickness of the selective coating, k_A is thermal conductivity of the selective coating, x is the arc length along the fin, U_L is the total loss coefficient, and T_b is the temperature at the point of contact between the pipe and the absorber fin.

The heat transfer by conduction at the point of contact between the fin and the pipe is calculated from Eq. 4,

$$q_{cond} = -k_A A_t m \lambda \tanh(m\pi D_{Ae}/2) \quad (4)$$

where $\lambda = T_b - T_\infty - S/U_L$.

2.1.3. Pipe

The energy collected at the fin is transferred to the working fluid as:

$$q_{cond} = (T_b - T_f)/R_{total} \quad (5)$$

where $T_f = (T_{in} + T_{out})/2$, T_{in} , T_{out} is the inlet and outlet temperature of the fluid, respectively, and R_{total} is the resistance by conduction and convection at the pipe given by Eq. 6 for the XCPC.

2.1.4. Thermal Resistance

The total thermal resistance from the pipe to the fluid is as follows:

$$R_{total} = \frac{\ln(D_{Oe}/D_o)}{2\pi L_D k_{Cu}} + \frac{1}{\pi D_o L_D h_{fluid}}, \quad (6)$$

where D_o is the inner diameter of the external copper pipe, D_{Oe} is the outer diameter of the external copper pipe, L_D is the length of the metal copper fin absorber, k_{Cu} is the thermal conductivity of copper, and h_{fluid} is the convection coefficient of the working fluid. The outlet temperature can be obtained from

$$q_{cond} = \dot{m} \cdot C_p \cdot \Delta T \quad (7)$$

where C_p is specific heat of the working fluid, $\Delta T = T_{out} - T_{in}$.

2.1.5. Efficiency

The efficiency, η , is calculated as,

$$\eta = \frac{q_{cond}}{A_{ge} \cdot G_s} \quad (8)$$

where A_{ge} is the area of the external glass wall.

2.2. Validation

The numerical model was validated with XCPC collector test data obtained by Winston et al. [16, 17] using Duratherm 600 thermal oil as the working fluid. Figure 3 shows the comparison of the thermal efficiency of the collector obtained from experimental data and numerical results for a range of inlet temperatures between 80 °C and 200 °C for a mass flow rate of thermal oil of 0.10 kg/s. The results agree reasonably well with the numerical model slightly under predicting the experimental data. Thus, by changing the thermophysical properties, it is possible to study the performance of such a collector using CO₂ as the working fluid. Carbon dioxide does require the operation at high pressure but this paper intends to analyze the thermal performance of such a working fluid so no stress analysis has been performed to adjust pipe wall thicknesses.

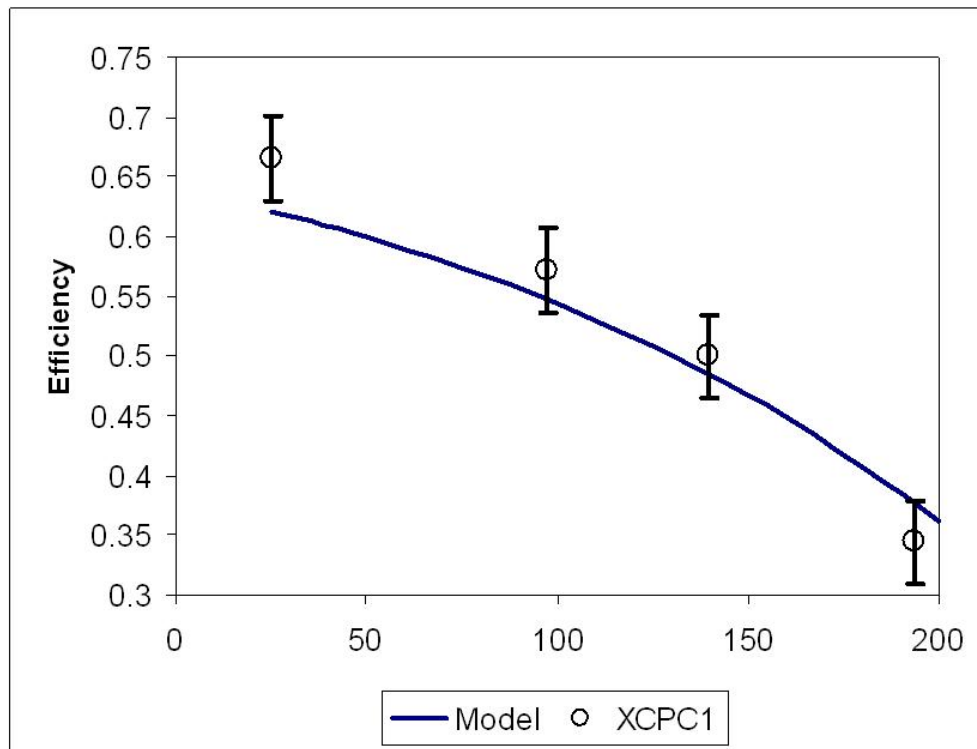


Figure 3. Validation of XCPC collector model with experimental test using Duratherm thermal oil at various input temperatures [17].

3. High Temperature: PTC

The concentration ratio, the effective aperture area to the glass area, is significantly higher in PTCs than in XCPC systems. The model used in this paper for the high-temperature parabolic trough concentrator with evacuated-tube absorber follows the analysis by Odeh et al. [7] which simulates the LS2 design developed by SEGS (Solar Thermal Electric Generation Systems). The evacuated-tube collector consists of a metal absorber concentric to a glass tube. Figure 4 depicts the cross-sectional view of the assembly. The working fluid directly flows from one end of the metal absorber tube to the other, i.e. single-pass configuration. The metal absorber in this model is made from steel with a total length of 99 meters. This total length is composed of 4-meter long collectors connected in series with metallic bellows at each end, to allow for the expansion of the metal absorber. The annulus between the glass tube and steel absorber is under vacuum and the external surface of the absorber pipe is covered with a selective coating. Input dimensions and parameters for PTC model are presented in Table 2.

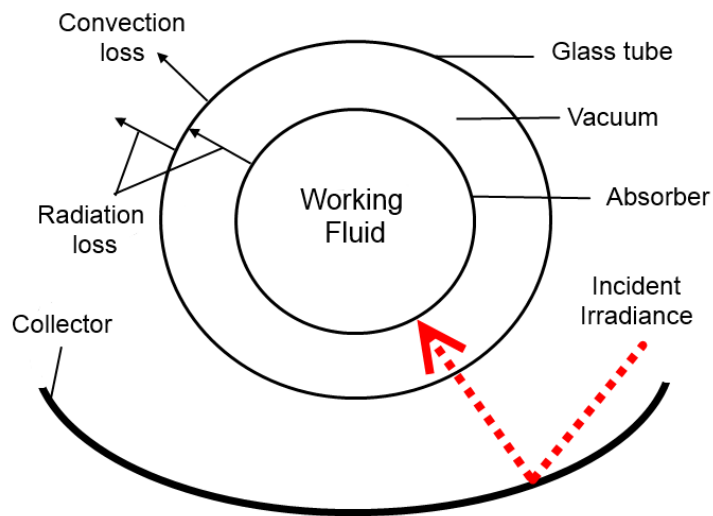


Figure 4. Model of the PTC with evacuated-tube absorber.

Table 2. Properties and Dimensions for PTC with Evacuated-Tube Absorber

Component	Symbol	Value
Glass tube		
Outer diameter	D_{ge}	115 mm
Inner diameter	D_g	109 mm
Thermal conductivity	k_g	1.4 W/m·K
Emissivity	ε_g	0.90
Evacuated-tube steel absorber		
Outer diameter	D_{Ae}	70 mm
Inner diameter	D_A	66 mm
Effective length	L_D	99 mm
Absorptivity	α_A	0.906
Selective coating		
Thermal conductivity	k_A	54 W/m·K
Thickness	t_0	1 mm

3.1. Mathematical Model of PTC

The mathematical model was implemented in EES to simulate the performance of the PTC with the metal pipe inside an evacuated-tube as described in Odeh et al. [7].

3.1.1. Glass Tube

The total heat loss of the glass tube, considering radiation from the glass to the sky, convection

from the glass to the surrounding air, and heat loss from the bellows, is given as:

$$q_{total,glass} = \sigma\epsilon_g(T_g^4 - T_{sky}^4)A_{ge} - h_0(T_g - T_\infty)A_{ge} - A_b h_0(T_A - T_\infty)\eta_b = 0 \quad (9)$$

where A_b is the exposed surface area of the bellows, η_b is the bellows fin efficiency which is estimated to be 70 %, and T_{sky} is adapted from [18] and approximated to be:

$$T_{sky} = T_\infty - 8. \quad (10)$$

3.1.2. Absorber

The total heat loss of the absorber due to radiation exchange between the absorber and glass and the convection from the bellows is:

$$q_{total,absorber} = \frac{\sigma(T_A^4 - T_g^4)}{\frac{1}{\epsilon_A}A_A - \frac{D_{Ae}}{D_g(1/\epsilon_g - 1)}} - h_0(T_A - T_\infty)\eta_b = 0 \quad (11)$$

where the emissivity of the absorber, ϵ_A is defined as,

$$\epsilon_A = 0.00042 \times T_{wall} - 0.0995 \quad (12)$$

and T_{wall} is the absorber wall temperature. Since we are assuming that the annulus, space between the glass and the absorber, is a perfect vacuum, the heat loss by conduction of the residual gas in the annulus is neglected.

The energy from absorber is transferred to the working fluid as:

$$q_{fluid} = \frac{T_A - T_{fluid}}{R_{total}} \quad (13)$$

where T_{fluid} is the temperature of the fluid and R_{total} is the resistance by conduction and convection of the PTC given by Eq. 14.

3.1.3. Thermal Resistance

The thermal resistance from the absorber pipe wall to the fluid has been calculated as follows:

$$R_{total} = \frac{\ln(D_{Ae}/D_A)}{2\pi L_D k_A} + \frac{1}{\pi D_A L_D h_{fluid}} \quad (14)$$

3.1.4. Efficiency

The efficiency formulation is obtained with the correlation provided by Odeh et al. [12]. The heat loss is given as

$$q = (a + c \cdot v) \cdot (T_A - T_\infty) + \epsilon_A (T_A^4 - T_{sky}^4) \quad (15)$$

where v is the wind velocity, and a , b , and c are coefficients. This formulation was developed to fit the LS2 collector type. This heat loss formulation is convenient since it depends solely on wind speed, absorber temperature, and ambient temperature. From Sandia National Laboratory testing on the LS2 collector, the parameters are $a = 1.9182 \times 10^{-2} \text{ W/m}^2 \cdot \text{K}$, $b = 2.02 \times 10^{-9} \text{ W/m}^2 \cdot \text{K}^4$, and $c = 6.612 \times 10^{-3} \text{ J/m}^3 \cdot \text{K}$.

The efficiency formulation can be expressed in terms of the heat loss formulation from Eq. 15. The development of the efficiency formulation is in terms of absorber temperature rather than working input temperature in order to consider performance of other working fluids. The efficiency is given by:

$$\eta = \eta_{opt} \cdot K_{\tau\alpha} - (a + c \cdot v) \cdot \frac{T_A - T_\infty}{I} - \epsilon_A \cdot b \cdot \frac{T_A^4 - T_{sky}^4}{I} \quad (16)$$

where η_{opt} is the optical efficiency of the collector, I is solar irradiance, and $K_{\tau\alpha}$ is the incident angle modifier. From LS2 collector tests ran by Dudley et al. [19], η_{opt} is given as 73.3 % where incident angle modifier is

$$K_{\tau\alpha} = \cos(\theta) + 0.000994(\theta) - 0.00005369(\theta)^2 \quad (17)$$

where θ is the beam incidence angle to the collector normal.

3. Results and Discussion

3.1. XCPC

Three cases were simulated to assess the performance of CO₂ as the working fluid in the XCPC collector with a metal absorber. The ranges of values used for the operating parameters in the model are provided in Table 3.

The first case analyzes the thermal efficiency of the collector as a function of working fluid inlet temperature for the range between 50 °C and 220 °C at three different mass flow rates (0.01, 0.02, and 0.03 kg/s). Figure 5 shows that efficiencies higher than 40 % can be obtained at operating temperatures near 200 °C. It is observed that the thermal efficiency is not a strong function of the mass flow rate for the range of values considered in this simulation.

The second case, presents the analysis of the thermal efficiency as a function of inlet temperatures of CO₂ at three different operating pressures, i.e. 9, 10, and 12 MPa. Figure 6, shows that the effect of operating pressure on the thermal efficiency is negligible for the three values of operating pressures modeled. Further reduction in pressure will cause a significant reduction in density of the working fluid so very high flow velocities would be required to maintain a fixed mass flow rate.

Lastly, the third case analyzes the effect of solar irradiance on the difference between outlet and inlet fluid temperature ($\Delta T = T_{out} - T_{in}$) to the collector. Solar irradiance covers the range between 300 and 1,000 W/m² for three different pressures (8, 9 and 10 MPa). Figure 7 indicates that ΔT varies linearly with solar irradiance for the range of values considered in this simulation. A reduction in operating pressure decreases the density of the working fluid resulting in a larger temperature difference, especially at high values of solar irradiance.

Table 3. XCPC – Simulated Cases

Case 1: Efficiency vs. input temperature at different flow rates	
Parameter	Range/Values
Temperature	50 °C to 220 °C
Flow rate, \dot{m}	0.01, 0.02, 0.03 kg/s
Solar irradiance	900 W/m ²
Case 2: Efficiency vs. input temperature at different pressures	
Parameter	Range/Values
Temperature	50 °C to 220 °C
Pressure, P	8, 9, 10 MPa
Solar irradiance	900 W/m ²
Case 3: ΔT vs. solar irradiance at different pressures	
Parameter	Range/Values
Solar irradiance	300 - 1000 W/m ²
Pressure, P	8, 9, 10 MPa
Inlet temperature	150 °C

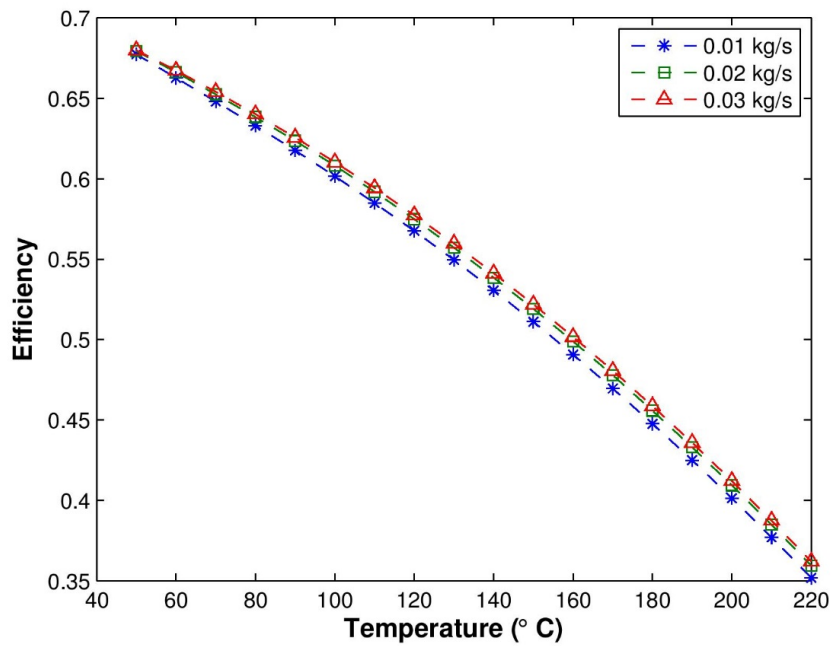


Figure 5. Thermal efficiency of XCPC with metal absorber for a range of inlet fluid temperatures between 50 °C and 200 °C, for three different mass flow rates of: 0.01 kg/s, 0.02 kg/s, and 0.03 kg/s and fixed value of pressure of 10 MPa.

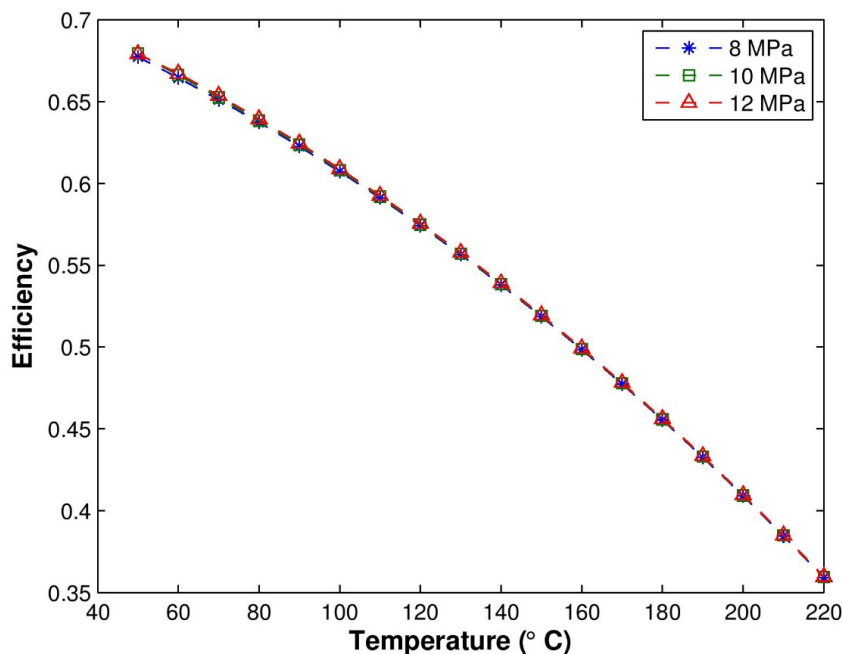


Figure 6. Thermal efficiency of XCPC with metal absorber for a range of inlet fluid temperatures between 50 °C and 200 °C, for three different operating pressures of CO₂: 8 MPa, 10 MPa, and 12 MPa and fixed mass flow rate of 0.01 kg/s.

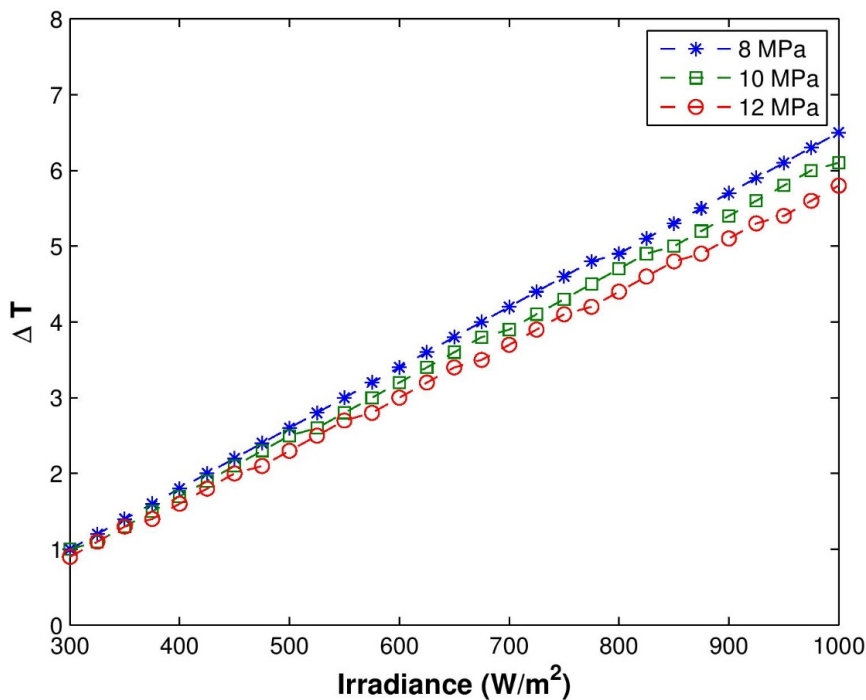


Figure 7. Variation between outlet and inlet fluid temperature ($\Delta T = T_{out} - T_{in}$) for an XCPC collector with metal absorber for an inlet temperature of $T_{in} = 150$ °C. The range of solar irradiation varies between 300 to 1000 W/m^2 and three different operating pressures of CO_2 have been simulated: 8 MPa, 10 MPa, and 12 MPa and for a fixed mass flow rate of 0.01 kg/s.

3.2. PTC

The analysis compares the overall heat loss of Syltherm 800 thermal oil and CO_2 for a range of fluid temperatures above ambient, i.e. $T_{fluid} - T_{\infty}$. The ranges of values used for the operating parameters in the model are provided in Table 4. Because of the properties of Syltherm 800, the maximum physical operable temperature is 400 °C. From Figure 8, it is seen that below 400 °C, the heat loss using CO_2 is comparable to Syltherm 800 at the same mass flow rate of 0.8 kg/s. The main difference is that the thermophysical properties of CO_2 remain stable so the simulation can be extended to a range of ΔT near 600 °C.

Due to the high operating pressure, it is desirable to minimize the CO_2 charge on the system. Thus, it is of interest to study the effect of lower mass flow rates on the total heat loss. Figure 8, shows total heat loss as a function of CO_2 mass flow rate for 0.8 kg/s, 0.2 kg/s and 0.08 kg/s. It is observed that at 600 °C above ambient temperature, the total heat loss for the CO_2 system increased approximately 10 % at 0.2 kg/s and 20 % at 0.08 kg/s compared to the heat loss at a mass flow rate of 0.8 kg/s.

Table 4. PTC – Simulated Case

Heat loss vs. ΔT for CO ₂ and Syltherm 800	
$T_{fluid} - T_{\infty}$	CO ₂ : 50 °C to 600 °C, Syltherm 800: 50 °C to 400 °C
Flow rate, \dot{m}	CO ₂ : 0.08, 0.2, and 0.8 kg/s, Syltherm 800: 0.8 kg/s
Pressure, P	CO ₂ : 12 MPa
Solar irradiance	1000 W/m ²

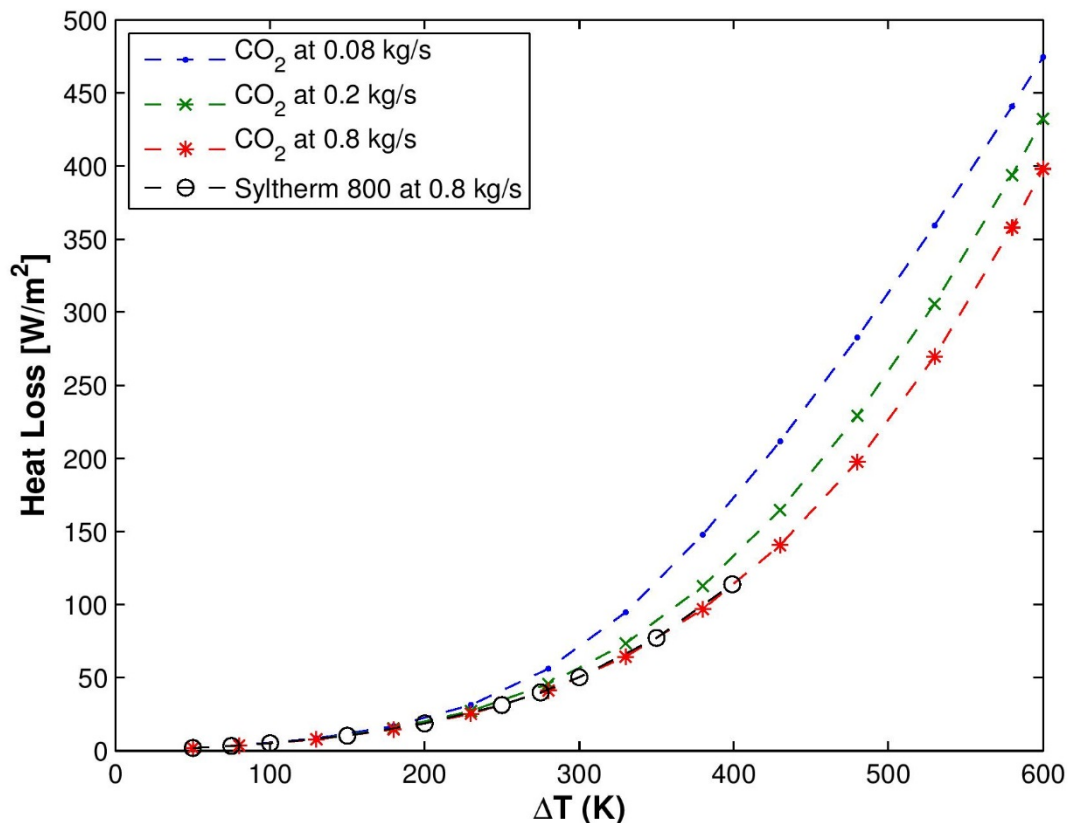


Figure 8. Total heat loss for a PTC with evacuated-tube absorber for a range of fluid temperatures above ambient between 50 °C and 600 °C. Mass flow rates of 0.08, 0.2, and 0.8 kg/s was used for CO₂, and 0.8 kg/s for Syltherm 800 with a set pressure of 12 MPa for CO₂.

4. Conclusions

In this study, two models of solar thermal collectors were implemented to analyze the performance of CO₂ as a working fluid. The model of the XCPC with metal absorber, for medium operating temperatures, shows that thermal efficiencies comparable to thermal oils can be achieved using CO₂ as the working fluid. The main drawback is the high operating pressure needed. For the

model of the PTC with evacuated-tube absorber, for high operating temperatures, the heat losses using CO₂ were also comparable to the ones obtained using Syltherm 800 but due to the thermal stability of carbon dioxide, a much larger range of fluid temperatures above ambient can be analyzed.

Acknowledgments

This project has been partially funded by the California Energy Commission, Contract#: POEF01-M04.

Nomenclature

A_{ge}	Area of the external glass wall, [m^2]
A_t	Cross-sectional area of the absorber fin, [m^2]
C_{max}	Concentration ratio of reflectors
C_p	Specific heat of working fluid, [$J/kg \cdot K$]
D_A	Inner diameter of the metal absorber, [m]
D_{Ae}	Outer diameter of the metal absorber, [m]
D_g	Inner diameter of the glass tube, [m]
D_O	Inner diameter of the external pipe, [m]
D_{Oe}	Outer diameter of the external pipe, [m]
G_c	Total irradiance incident on the absorber, [W/m^2]
G_S	Solar irradiance incident on concentrator aperture, [W/m^2]
h_0	Convection coefficient on outside of glass cover, [$W/m^2 \cdot K$]
h_{fluid}	Convection coefficient of working fluid, [$W/m^2 \cdot K$]
I	Solar irradiance, [W/m^2]
k_A	Thermal conductivity of the selective coating on the metal absorber, [$W/m \cdot K$]
k_{Cu}	Thermal conductivity of copper pipe, [$W/m \cdot K$]
$K_{\tau\alpha}$	Incident angle modifier
L_D	Effective length of the absorber, [m]
\dot{m}	Mass flow rate of working fluid, [kg/s]
q	Heat transfer, [W]
q''	Heat flux, [W/m^2]
R_{total}	Total thermal resistance from the external wall of the pipe to the fluid, [m]
t_0	Thickness of selective coating, [m]
T	Temperature of working fluid, [K]
T_A	Temperature of absorber, [K]
T_b	Temperature of the fin at contact point with the external copper pipe, [K]
T_{fluid}	Temperature of the working fluid, [K]
T_g	Temperature of glass cover, [K]
T_{in}	Inlet temperature of working fluid, [K]
T_{out}	Outlet temperature of working fluid, [K]
T_{sky}	Temperature of atmosphere, [K]
T_{wall}	Absorber wall temperature, [K]
T_{∞}	Temperature of ambient air, [K]

v	Wind velocity, [m/s]
x	Arc length of absorber fin, [m]
<i>Greek Symbols</i>	
α_A	Absorptivity of the absorber
α_g	Absorptivity of the glass
ε_A	Emissivity of the metal absorber
ε_g	Emissivity of the glass
τ_g	Transmissivity of glass
ρ_g	Reflectivity of glass
η	Efficiency of the collectors
η_b	Fin efficiency of the bellows
η_{opt}	Optical efficiency of the collectors
κ	Absorption coefficient of absorber fin

References

1. Chen Y, Pridasawas W, Lundqvist P (2010) Dynamic simulation of a solar-driven carbon dioxide transcritical power system for small scale combined heat and power production. *Solar Energy* 84: 1103-1110.
2. Yamaguchi H, Zhang X, Fujima K, et al. (2006) Solar energy powered rankine cycle using supercritical CO₂. *Appl Therm Eng* 26: 2345-2354.
3. Kim MH, Pettersen J, Bullard CW (2004) Fundamental process and system design issues in CO₂ vapor compression systems. *Prog Energy Combust* 30: 119-174.
4. Liu J, Chen H, Xu Y, et al. (2014) A solar energy storage and power generation system based on supercritical carbon dioxide. *Renew Energ* 64: 43-51.
5. Winston R (1974) Principles of solar concentrators of a novel design. *Sol Energ* 16: 89-95.
6. Kim YS, Balkoski K, Jiang L, et al. (2013) Efficient stationary solar thermal collector systems operating at a medium-temperature range. *Appl Energ* 111: 1071-1079.
7. Odeh S, Morrison G, Behnia M (1998) Modeling of parabolic trough direct steam generation solar collectors. *Sol Energ* 62: 395-406.
8. Tamme R, Laing D, Steinmann WD (2004) Advanced thermal energy storage technology for parabolic trough. *J Sol Energ Eng* 126: 794-800.
9. Price H, Lufert E, Kearney D, et al. (2002) Advances in parabolic trough solar power technology. *J Sol Energ Eng* 124: 109-125.
10. Montes MJ, Abanades A, Martinez-Val JM (2010) Thermofluidynamic model and comparative analysis of parabolic trough collectors using oil, water/steam, or molten salt as heat transfer fluids. *J Sol Energ Eng* 132: 1-7.
11. Guyer EC. (1999) Handbook of Applied Thermal Design. In: Taylor, Francis.
12. Trovar-Fonseca A (2008) Performance assessment of three concentrating solar thermal units designed with XCPC reflectors and evacuated tubes, using an analytical thermal model. Master's thesis, University of California, Merced.
13. Duffe JA, Beckman WA (1999) Solar Engineering of Thermal Processes. Inc., 3rd edition. John Wiley & Sons.
14. Klien SA. Engineering Equation Solver (EES) [Ver. 9.433]. F-Chart Software, Madison.

15. Khoukhi M, Maruyama S (2005) Theoretical approach of a flat plate solar collector with clear and low-iron glass covers taking into account the spectral absorption and emission within glass covers layer. *Renew Energ* 30: 1177-1194.
16. Winston R, Diaz G, Ritzel A, et al. (2009) High temperature CPC collectors with chinese vacuum tube receivers. In: Goswami D. and Zhao Y. (eds.), *Proceedings of ISES World Congress 2007* (Vol. I - Vol. V), Springer Berlin Heidelberg, 661-662.
17. O’Gallagher JJ, Winston R, Gee R (2006) Continuing development of high-performance low-cost XCPC. *Proceedings of ASME International Solar Energy Conference, Solar 2006 Vol. I – Vol. III*: 66-72.
18. Wirz M, Roesle M, Steinfeld A (2012) Three-dimensional optical and thermal numerical model of solar tubular receivers in parabolic trough concentrators. *J Sol Energ Eng* 234: 041012:1-9.
19. Dudley V, Kolb G, Sloan M, et al. (1994) SEGS LS2 solar collector - test results. Report of Sandia National Laboratory, No. SANDIA94-1884.

© 2014, Gerardo Diaz, et al., licensee AIMS Press. This is an open access article distributed under the terms of the Creative Commons Attribution License (<http://creativecommons.org/licenses/by/4.0>)